Thermodynamics of the Interaction of the *Escherichia coli* Regulatory Protein TyrR with DNA Studied by Fluorescence Spectroscopy†

Michael F. Bailey,‡ Barrie E. Davidson,‡ Jim Haralambidis,§ Terry Kwok,‡ and William H. Sawyer*,‡

The Russell Grimwade School of Biochemistry and Molecular Biology, and The Howard Florey Institute of Experimental Physiology and Medicine, University of Melbourne, Parkville, Victoria 3052, Australia

Received November 20, 1997; Revised Manuscript Received March 6, 1998

ABSTRACT: Fluorescence quenching was used to study the site-specific binding of the *Escherichia coli* regulatory protein TyrR to a fluoresceinated oligonucleotide (9F30A/30B) containing a TyrR binding site. The equilibrium constant for the interaction (K_L) was measured as a function of temperature and salt concentration in the presence and absence of ATPγS, a specific ligand for TyrR. Fluorescence titrations yielded a K_L value of 1.20×10^7 M^{-1} at 20 °C, which was independent of the acceptor (9F30A/30B) concentration in the range 5−500 nM, indicating that the system exhibits true equilibrium binding. Clarke and Glew analysis of the temperature dependence of binding revealed a linear dependence of $R \ln K_L$ on temperature in the absence of ATPγS. The thermodynamic parameters obtained at 20 °C (θ) were $\Delta G^\circ_\theta = -35.73$ kJ mol^{-1}, $\Delta H^\circ_\theta = 57.41$ kJ mol^{-1}, and $T\Delta S^\circ_\theta = 93.14$ kJ mol^{-1}. Saturating levels of ATPγS (200 μM) strengthened binding at all temperatures and resulted in a nonlinear dependence of $R \ln K_L$ on temperature. The thermodynamic parameters characterizing binding under these conditions were $\Delta G^\circ_\theta = -39.32$ kJ mol^{-1}, $\Delta H^\circ_\theta = 37.16$ kJ mol^{-1}, $T\Delta S^\circ_\theta = 76.40$ kJ mol^{-1}, and $\Delta C^\circ_{p\theta} = -1.03$ kJ mol^{-1} K^{-1}. Several conclusions were drawn from these data. First, binding is entropically driven at 20 °C in both the presence and absence of ATPγS. This can partly be accounted for by counterions released from the DNA upon TyrR binding; in the absence of ATPγS and divalent cations, the TyrR−9F30A/30B interaction results in the release of two to three potassium ions. Second, the more favorable ΔG°_θ value, and hence tighter binding observed in the presence of ATPγS, is primarily due to a decrease in ΔH°_θ (−20.3 kJ mol^{-1}), which overcomes an unfavorable decrease in $T\Delta S^\circ_\theta$ (−16.7 kJ mol^{-1}). Third, the negative $\Delta C^\circ_{p\theta}$ value obtained in the presence of ATPγS indicates that the binding of ATPγS favors a conformational change in TyrR upon binding to 9F30A/30B, yielding a more stable complex.

The TyrR protein plays an integral role in the control of aromatic amino acid metabolism in *Escherichia coli* (*1*, *2*). TyrR regulates the expression of at least eight unlinked operons comprising the TyrR regulon, whose products are involved in aromatic amino acid biosynthesis and transport. It acts as a repressor of *aroFtyrA*, *aroLM*, *tyrB*, *aroP*, *tyrR*, and *aroG*, as an activator of *mtr*, and as either a repressor or an activator of *tyrP*. Repression varies considerably in magnitude between different operons (*3*, *4*) and is ATP-dependent, usually involving tyrosine as the corepressor, whereas activation is ATP-independent and requires any of the three aromatic amino acids.

TyrR exists as a homodimer in solution with a subunit molecular mass of 57 640 Da (*5*, *6*). Limited proteolysis experiments indicate that it has a multidomain structure (*7*). The N-terminal domain is implicated in transcriptional activation (*3*, *8*, *9*), its activity believed to be modulated by the binding of aromatic amino acids to an ATP-independent site within this domain (*10*). TyrR binds one mole of ATP per mole of subunit with half-maximal saturation at 5−7 μM (*5*). It is likely that the ATP binding site is located in the central domain, since this region of the protein has a significant degree of sequence homology with the ATP binding site in adenylate kinase and with sequences present in other prokaryotic regulatory proteins that bind ATP, such as NtrC, NifA, and XylR (*11*−*13*). Since the concentration of ATP in *E. coli* is maintained at about 3 mM (*14*), the ATP binding sites in TyrR should be saturated (*6*). ATP facilitates ATP-dependent aromatic amino acid binding at a site also thought to reside in the central domain. The C-terminal region of TyrR contains the DNA binding domain, which is predicted to form a helix-turn-helix motif similar to the DNA binding domains of other prokaryotic regulatory proteins, such as the catabolite activator protein, the *lac* repressor, and lambda cro (*3*).

The DNA sites to which TyrR binds (TyrR boxes) are characterized by the palindromic consensus sequence $TGTAAAN_6TTTACA$. Two classes of TyrR box have been

† Supported by grants from the Australian Research Council (to W.H.S. and B.E.D.). M.B. and T.K. are the recipients of Australian Postgraduate Research Awards.

* To whom correspondence should be addressed. Telephone: +61 3 93445923. Fax: +61 3 93447730. E-mail: w.sawyer@biochemistry.unimelb.edu.au.

‡ The Russell Grimwade School of Biochemistry and Molecular Biology.

§ The Howard Florey Institute of Experimental Physiology and Medicine.

S0006-2960(97)02854-7 CCC: $15.00
Published on Web 04/30/1998

identified. Strong boxes contain more than 10 bp[1] of the consensus sequence and bind TyrR in vitro in the absence of an aromatic amino acid coeffector. The affinity of TyrR for strong boxes is enhanced in the presence of ATP (*2*, *4*). Weak boxes have less identity with the consensus sequence and bind TyrR in vitro only in the presence of ATP and an aromatic amino acid and when there is an adjacent strong box (*2*, *15*−*17*). All operons except *aroG* possess a tandem strong/weak box pair usually separated (center-to-center) by 23 bp, with *aroFtyrA* and *aroLM* having an additional strong box centered approximately 50 bp upstream from the weak box (*2*). In most operons repressed by tyrosine, overlap of the promoter by the operator is predominantly via the weak box.

It has been suggested that transcriptional regulation of the TyrR regulon is primed by the permanent occupancy of strong boxes by the TyrR dimer−ATP complex (*6*), with the levels of aromatic amino acid coeffectors modulating TyrR activity. Analyses of insertion mutants of the *tyrP* and *aroFtyrA* operators suggest that tyrosine-mediated repression requires protein−protein interactions between TyrR molecules bound to adjacent boxes (*18*). The observation that TyrR self-associates from dimer to hexamer in the presence of ATP (or the nonhydrolyzable analogue ATPγS) and tyrosine has led to a model incorporating the hexamerization of TyrR in situ on the operator DNA to explain tyrosine-mediated repression (*6*). As part of this model it was postulated that the upstream boxes in the *aroFtyrA* and *aroLM* operons can associate with the downstream hexamer−DNA complex via DNA looping, thereby yielding a tighter interaction. In contrast to the disposition of TyrR boxes required for tyrosine-mediated repression, only the strong box is required for phenylalanine-mediated activation of *tyrP* and *mtr* (*15*, *18*), suggesting that self-association is not required to bring about this activity. Presumably, the TyrR dimer, with phenylalanine bound at the ATP-independent site, is the species responsible for phenylalanine-mediated activation (*10*).

Notwithstanding the extensive data concerning the interaction of TyrR with DNA obtained by molecular genetic approaches, there is little known about this area at the thermodynamic level. We have shown previously that conjugation of a fluorescent probe at particular bases within the consensus sequence can be used to footprint the interaction site on the DNA and to determine the equilibrium constant for the interaction with TyrR (*19*, *20*). In this paper we report the use of one such conjugate to study the thermodynamics of the TyrR-DNA interaction and to define the contribution ATP makes to the energetics of site-specific TyrR-DNA binding.

EXPERIMENTAL PROCEDURES

Materials. FITC (isomer I) was from Molecular Probes, Oregon. ATPγS was from Boehringer (Mannheim, Germany). β-Cyanoethyl phosphoramidites were from Applied Biosystems. All other reagents were of analytical grade.

[1] Abbreviations: bp, base pair(s); FITC, fluorescein-5-isothiocyanate; ATPγS, adenosine-5′-*O*-(3-thiotriphosphate); HPLC, high-pressure liquid chromatography; SDS, sodium dodecyl sulfate; PAGE, polyacrylamide gel electrophoresis; fwhm, full width at half-maximum; TBE, Tris, boric acid, and EDTA.

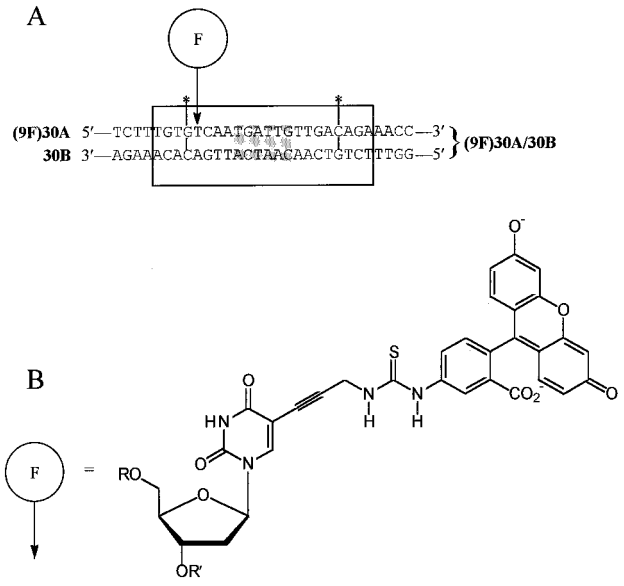

FIGURE 1: Nucleotide sequences and features of oligonucleotide 30mers used for TyrR binding studies. Part A shows the nucleotide sequences of the complementary oligonucleotides 30A (top strand) and 30B (bottom strand) that form the duplex 30A/30B, the sequence of which corresponds to base pairs 224−253 of the *tyrR* gene (*40*). The 22 bp enclosed by the rectangle comprise the strong TyrR box (TyrR binding site), which has an approximate 2-fold axis of symmetry about the central N_6 region (shaded). The GC basepairs marked by the symbol * are conserved throughout all TyrR boxes and are essential for TyrR activity (*2*). The circled letter F indicates that thymine residue 9 of 30A was replaced with a 5-(3-aminoprop-1-yn-1-yl)-2′-deoxyuridine residue and subsequently labeled with FITC. In this case, 30A is known as 9F30A and the duplex as 9F30A/30B. Part B shows the structure of the fluorescein-labeled 5-(3-aminoprop-1-yn-1-yl)-2′-deoxyuridine residue. The fluorescein moiety, attached to the DNA via a thiocarbamide function, is drawn in its predominant (dianionic) form at pH 7.4 (*41*).

Oligonucleotide Synthesis, Purification, and Labeling. Complementary oligonucleotides, designated 30A and 30B (containing the strong box from the *tyrR* operator, Figure 1), were synthesized, HPLC purified, and transferred into buffer F (100 mM KCl, 25 mM K_2HPO_4 pH 7.4 adjusted with HCl, 1 mM EDTA, 0.1 mM DTT, 0.02% NaN_3) as described previously (*19*, *20*). Oligonucleotide concentrations were determined at 260 nm using molar extinction coefficients of 3.41×10^5 M^{-1} cm^{-1} for 30A and 3.47×10^5 M^{-1} cm^{-1} for 30B, these values being calculated from their nucleotide sequences (*21*). Equimolar amounts of each strand were mixed, and the solution was incubated at 90 °C for 5 min, then cooled to room temperature at 0.5 °C/min to give the double-stranded oligonucleotide, 30A/30B. In a separate synthesis, the thymine residue at position 9 from the 5′ end of 30A was replaced by a 5-(3-aminoprop-1-yn-1-yl)-2′-deoxyuridine residue (Figure 1) (*19*). The modified oligonucleotide was FITC labeled, HPLC purified and transferred into buffer F as described previously (*19*, *20*). The labeling ratio of the 9F30A conjugate was 1.1 fluorescein molecules/30mer based on extinction coefficients for the fluorescein chromophore of 2.4×10^4 M^{-1} cm^{-1} at 260 nm and 7.2×10^4 M^{-1} cm^{-1} at 495 nm (*19*, *22*). 9F30A was annealed to 30B as above to produce the duplex 9F30A/30B (Figure 1). The molar concentration of 9F30A/30B was determined at 260 nm using an extinction coefficient of 5.3

$\times 10^5$ M^{-1} cm^{-1}, which accounts for a 30% reduction in the absorption at this wavelength due to hypochromicity (*19*).

TyrR Preparation. TyrR protein was prepared as described (*5*), with the inclusion of an extra step between phosphocellulose P11 and Superose 12 chromatography (*10*). In this step gel permeation chromatography was carried out with the eluent (buffer F) containing saturating concentrations of ATP (200 μM) and tyrosine (1 mM). This enables the isolation of TyrR molecules that are fully active with respect to hexamerization and therefore ATP binding and ATP-dependent aromatic amino acid binding. The preparation was greater than 95% pure as judged by SDS−PAGE, with a yield of 25 mg/L of culture. The concentration of TyrR was determined spectrophotometrically at 280 nm using an extinction coefficient of 3.45×10^4 M^{-1} cm^{-1} $monomer^{-1}$ (*19*) and is expressed on a dimer basis.

Thermal Denaturation of Oligonucleotide 30mers. Melting curves were measured on a CARY 5 spectrophotometer fitted with thermal accessories. Samples were measured at 260 nm at a heating rate of 1 °C/min. The solution temperature was monitored with a thermocouple probe inserted into a cuvette containing buffer F, adjacent to the sample in the thermostated cell block. The transition melting temperature (T_m) was obtained from the midpoint of the denaturation curve.

Fluorescence Spectra and Titrations. Fluorescence measurements were made on a SPEX Fluorolog-τ2 instrument with 3 mL capacity Teflon-stoppered cells. Spectra were recorded at 1 nm/min using excitation and emission wavelengths of 490 and 515 nm, respectively, with slit widths of 2.5 nm (fwhm). The quenching of 9F30A/30B fluorescence upon TyrR binding was used to determine the binding constant for the interaction. In a typical titration, a 2 mL, 50 nM solution of 9F30A/30B (in buffer F plus 10 mM $MgCl_2$, ± 200 μM ATPγS) was titrated with aliquots of TyrR. ATPγS, a nonhydrolyzable analogue of ATP (*23*), was used in these experiments to avoid ATP hydrolysis catalyzed by the weak ATPase activity of TyrR (*24*). After each addition of TyrR, the solution was mixed by gentle inversion, returned to the cell block, and left for at least 10 min to equilibrate to the experimental temperature, by which time a stable fluorescence reading was obtained. The solution temperature was monitored as described in the previous section. Fluorescence intensities at each point in the titration were measured at the wavelengths above and were the average of four readings that were themselves integrated over a period of 20 s. Data were then corrected for volume dilution and for background fluorescence (typically less than 0.1% of the total signal). To ensure that dilution of the 9F30A/30B solution was not greater than 10% at the endpoint of a titration, more concentrated TyrR stocks were used after the solution had been diluted by 5% and 7.5%, respectively. Each new stock solution was 3−5-fold more concentrated than the previous one.

For titrations in the presence and absence of ATPγS at different temperatures, 9F30A/30B was diluted to a concentration of 50 nM in 50 mL of buffer F. Two portions of approximately 19 mL were aliquoted into 20 mL standard flasks, with ATPγS (40 μL, 200 μM) added to one and the same volume of buffer F added to the other. Both flasks were made up to 20 mL with the original 9F30A/30B solution and the stocks stored at −20 °C. Titrations were performed with 2 mL aliquots of these solutions supplemented with 10 mM $MgCl_2$.

Buffers I and J were prepared for titrations at different KCl concentrations: the composition of each buffer was identical to that of buffer F except that the concentration of KCl was 25 and 145 mM, respectively. Both buffers were adjusted to pH 7.4 and mixed to provide buffers with the desired potassium ion concentrations. 9F30A/30B was diluted to a concentration of 50 nM in 4.2 mL of the appropriate buffer and aliquoted into 2 mL portions for titrations. When required, $MgCl_2$ and ATPγS were added to concentrations of 10 mM and 200 μM, respectively.

Gel Shift Titrations. Reaction mixtures were made up to 20 μL in buffer F and comprised 9F30A/30B or 30A/30B (0.5 μM), ATPγS (200 μM), $MgCl_2$ (10 mM), glycerol (10% v/v), and TyrR (from 0 to 5 μM). When ATPγS was not required, it was replaced by buffer F. Ten microliters of each mixture was electrophoresed on a 7.5% polyacrylamide gel in 1 × TBE for 1 h at a 15 mA constant current. Gels were stained in 1 μg/mL ethidium bromide for 10 min, destained in distilled water for 5 min, placed on a UV transilluminator, and photographed.

Circular Dichroism Spectroscopy. CD spectroscopy was performed on an Aviv Model 62 DS instrument with 0.1 cm path length quartz cuvettes. Unless otherwise stated, data were collected at 0.5 nm/min and at 20 °C. Separate spectra of 30A/30B (10 μM) and TyrR (50 μM) in buffer F plus 10 mM $MgCl_2$ were recorded in triplicate, averaged, and corrected against buffer F/$MgCl_2$. Spectra were offset to 0 mdeg in the region 310−340 nm (where neither species displays ellipticity), then smoothed using a 7 point window. To examine changes in the DNA structure accompanying TyrR binding, a mixture containing 30A/30B and TyrR at the above concentrations was measured. In this case, the corrected spectrum was obtained by subtracting the CD spectrum of TyrR in buffer F/$MgCl_2$ from that of the mixture. The corrected spectrum was then treated as above. Data were collected and analyzed in a fashion identical to that above when solutions also contained 200 μM ATPγS.

RESULTS

Binding of TyrR to 9F30A/30B. Preliminary experiments showed that the fluorescein fluorescence of 9F30A/30B was quenched upon the addition of TyrR. To determine whether the quenching can provide a quantitative measure of the binding equilibrium, the 9F30A/30B acceptor was prepared at concentrations of 5, 50, and 500 nM, and each solution was titrated with TyrR (Figure 2, parts A, B, and C, respectively). The binding constant for the interaction, K_L, was obtained by a global fit of the three isotherms to eq 4, which assumes a 1:1 stoichiometry for the TyrR−9F30A/30B complex (see Appendix). In each case, the data are well described by a single K_L value of $1.20 \pm 0.06 \times 10^7$ M^{-1} (continuous lines). This compares favorably with the analysis of individual isotherms, where the best-fit values of K_L were $1.03 \pm 0.01 \times 10^7$, $1.22 \pm 0.02 \times 10^7$, and $1.20 \pm 0.01 \times 10^7$ M^{-1} at acceptor concentrations of 5, 50, and 500 nM, respectively. The fact that K_L is independent of the acceptor concentration confirms the equilibrium nature of the binding system. Implicit in this treatment is the assumption that all of the protein is competent in binding to

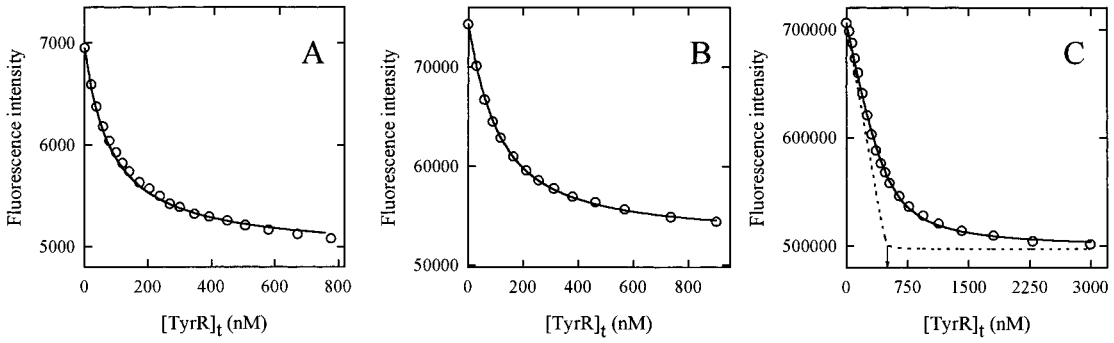

FIGURE 2: Fluorescence titrations of DNA with TyrR. Solutions containing 9F30A/30B at concentrations of 5 nM (A), 50 nM (B), and 500 nM (C) were titrated with TyrR, at 20 °C in the presence of ATPγS (200 μM) and $MgCl_2$ (10 mM). The fluorescence intensity (○) is plotted against the total concentration of TyrR added. The continuous lines are the best global fit of the data to eq 4, which yields a value of 1.20×10^7 M^{-1} for the binding constant K_L (see Appendix). The dotted line in Figure 2C is a simulated titration of a 1:1 interaction of 9F30A/30B (500 nM) with TyrR. The line was generated by assigning a value of 1.20×10^9 M^{-1} for K_L and by assuming the same degree of fluorescence quenching as seen in the experimental data. The downward arrow corresponds to a TyrR concentration of ~520 nM.

9F30A/30B. The legitimacy of this assumption was tested by further analysis of the data in Figure 2C. Under the conditions of this experiment, the binding approaches the stoichiometric limit due to the 9F30A/30B concentration being 6-fold higher than the K_d for the interaction ($1/K_L$). Thus, for TyrR that is completely active in binding to DNA, the experimental data should mirror a stoichiometric binding isotherm at low binding occupancy (<10%). To facilitate this comparison, a simulated stoichiometric binding curve was generated by increasing the value of K_L by 2 orders of magnitude (1.20×10^9 M^{-1}) and using the same variables as used to fit the experimental data (Figure 2C, dotted line). The stoichiometric end point of this curve corresponds to a TyrR concentration of ~520 nM (Figure 2C, downward arrow), a concentration very near that of 9F30A/30B used in this experiment (500 nM). The close agreement between the experimental and simulated data sets at low binding occupancy suggests that the TyrR prepared for this study possesses full DNA-binding activity.

The optimal conditions for determining the effect of temperature and salt concentration on the binding of TyrR to 9F30A/30B (see below) are those used in Figure 2B where the acceptor concentration is close to the K_d for the interaction. At higher acceptor concentrations, the binding becomes more stoichiometric, whereas at lower acceptor concentrations, errors due to background fluorescence and light-scattering artifacts become more problematic. Having established conditions for studying the thermodynamics of TyrR−9F30A/30B binding, a larger quantity of the labeled oligonucleotide was prepared.

Thermal Stability of Oligonucleotides and TyrR. The thermal stabilities of the oligonucleotide 30mers and TyrR were examined to determine the temperature range over which the binding equilibrium could be examined (Figure 3). Oligonucleotide melting was monitored spectrophotometrically by making use of the hyperchromicity at 260 nm (Figure 3A). The A_{260} nm data were converted to percent denaturation assuming the 30mers to be fully native at 15 °C and fully denatured at 85 °C. Analysis of the melting curves by the two-state midpoint method of Breslauer and co-workers (*25*) gave transition melting temperatures (T_m) of 61.4 and 65.3 °C for 9F30A/30B and 30A/30B, respectively, values that agreed with those obtained by first derivative analysis of the A_{260} nm data (not shown). While

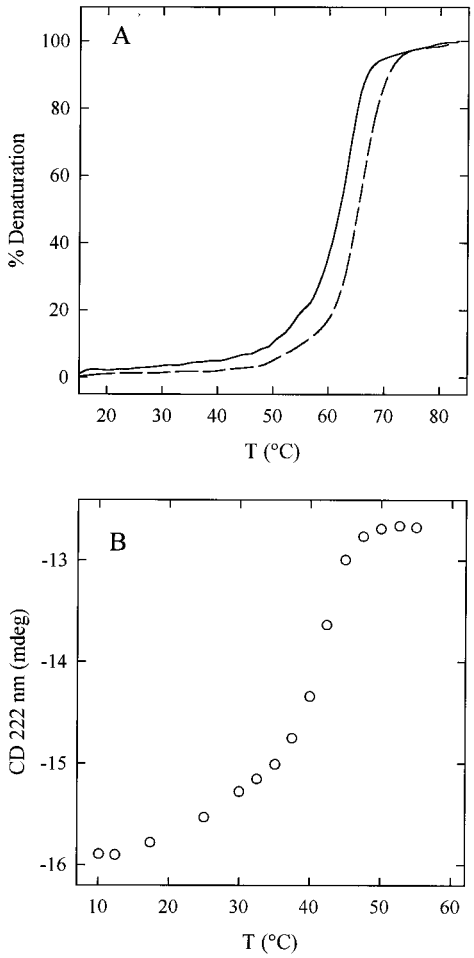

FIGURE 3: Thermal denaturation of DNA and TyrR. Part A: normalized melting curves for 0.4 μM 9F30A/30B (—) and 0.7 μM 30A/30B (– – –) in buffer F. A_{260} nm data were converted to percent denaturation assuming the duplexes were fully native at 15 °C and fully denatured at 85 °C. The transition melting temperatures for 9F30A/30B (61.4 °C) and 30A/30B (65.3 °C) were obtained from the midpoints of their respective melting curves. Part B: thermal denaturation of TyrR monitored by circular dichroism at 222 nm. TyrR (1.6 μM in buffer F) was measured in a 0.1 cm path length cuvette over the temperature range 10−55 °C. For each temperature point, the data were averaged for 5 min and corrected against buffer F.

the introduction of the negatively charged fluorescein dye into a negatively charged polyelectrolyte destabilized 9F30A/

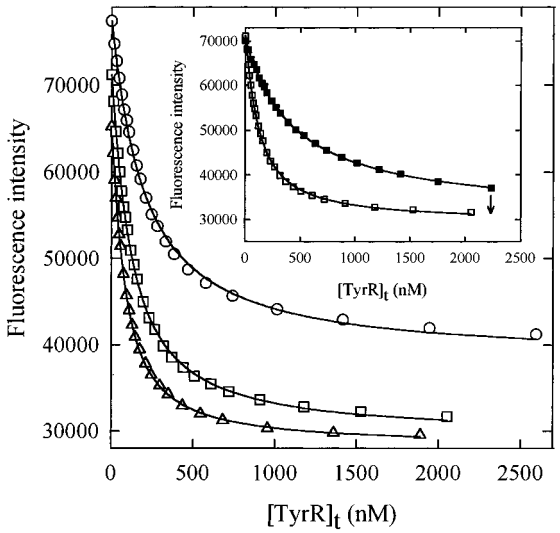

FIGURE 4: Temperature dependence of the interaction of TyrR with DNA. Solutions of 9F30A/30B (50 nM) were titrated with TyrR at 10 (○), 20 (□), and 35 °C (△) in the presence of ATPγS (200 μM) and $MgCl_2$ (10 mM). Inset: titration of 9F30A/30B with TyrR at 20 °C as above (□) and in the absence of ATPγS (■). The downward arrow indicates that the addition of 200 μM ATPγS resulted in the fluorescence intensity measured for the titration conducted in the presence of ATPγS. The continuous lines in both sections are the best fit of each titration curve to eq 4 with the K_L values presented in Table 1.

30B relative to 30A/30B, more than 95% of the labeled oligonucleotide remained intact up to temperatures of 40 °C.

The increase in circular dichroism ellipticity at 222 nm, representing the change from α-helix to unordered structure, was used to follow the thermal denaturation of TyrR (Figure 3B). TyrR denaturation was described by a single transition between 10 and 55 °C, with a T_m of 40 °C determined from the midpoint of the transition. A further increase in ellipticity was observed from 60 to 85 °C which coincided with the precipitation of TyrR (data not shown). On the basis of these data and the observation that the rate of ATP hydrolysis by TyrR is maximal at 37 °C,[2] the upper limit for studying the effect of temperature on binding was set at 35 °C. This temperature should provide the largest window for the thermodynamic analysis of TyrR−DNA binding, at the same time ensuring that both macromolecules retain their structural integrity.

Effect of Temperature on the Binding of TyrR to DNA. Fluorescence titrations were conducted in the presence and absence of ATPγS over the temperature range 5−35 °C to investigate the thermodynamics of the TyrR-DNA interaction. It was assumed that the concentration of ATPγS used (200 μM) was sufficient to saturate the ATP binding sites on the TyrR dimer at all temperatures. The temperature dependence of the interaction in the presence of ATPγS is illustrated by the titration curves presented in Figure 4. Fitting the data to eq 4 provided association constants of 5.76×10^6, 1.01×10^7, and 1.71×10^7 M^{-1} at 10, 20, and 35 °C, respectively (Table 1). Although the fluorescence intensity of 9F30A/30B in the absence of TyrR varied inversely with increasing temperature, the quenching of fluorescence due to TyrR binding was relatively independent of temperature, being approximately 59%.

[2] Personal communication, Peter Maroudas, The Russell Grimwade School of Biochemistry and Molecular Biology, University of Melbourne, Parkville, Victoria, Australia.

Table 1: Temperature Dependence of the Binding Constant for the Interaction of TyrR with 9F30A/30B[a]

	K_L[b] (M^{-1})		
temperature (°C)	+ATPγS[c]	−ATPγS	ratio[d]
5	$3.68 \pm 0.13 \times 10^6$	nd[e]	
10	$5.76 \pm 0.14 \times 10^6$	$1.11 \pm 0.04 \times 10^6$	5.2
15	$7.30 \pm 0.14 \times 10^6$	$1.41 \pm 0.04 \times 10^6$	5.2
20	$1.01 \pm 0.01 \times 10^7$	$2.35 \pm 0.02 \times 10^6$	4.3
25	$1.21 \pm 0.03 \times 10^7$	$3.14 \pm 0.06 \times 10^6$	3.9
30	$1.67 \pm 0.02 \times 10^7$	$5.13 \pm 0.07 \times 10^6$	3.3
35	$1.71 \pm 0.02 \times 10^7$	$7.16 \pm 0.08 \times 10^6$	2.4

[a] All measurements were made in buffer F (see Experimental Procedures) containing 10 mM $MgCl_2$. [b] Binding constants (K_L) were obtained by fitting fluorescence titration data to eq 4 (see Appendix). [c] ATPγS was present at a concentration of 200 μM. [d] The ratio equals K_L(+ATPγS)/K_L(−ATPγS). [e] Not determined due to the low binding affinity at this temperature.

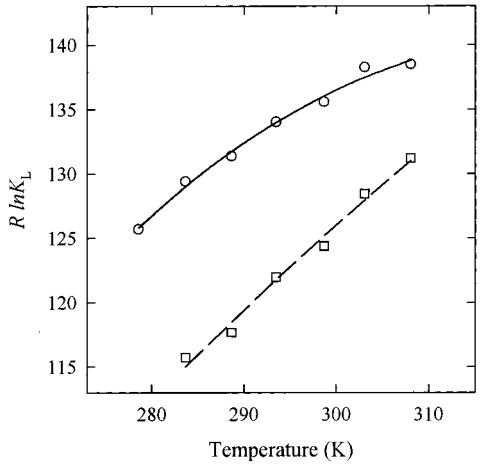

FIGURE 5: Thermodynamic analysis of TyrR-DNA binding. The K_L values shown in Table 1 were converted to the product of the gas constant and their natural logarithm ($R \ln K_L$) and plotted as a function of the absolute temperature. The data obtained in the presence (○) and absence (□) of ATPγS were fitted to the Clarke and Glew equation (see Appendix) about the reference temperature 293.15 K (20 °C). The standard heat capacity change at constant pressure ($\Delta C^\circ_{p\theta}$) was either used as a fitting parameter (—) or constrained to zero (− − −).

The inset to Figure 4 shows that the binding of ATPγS to TyrR increases the DNA binding affinity by a factor of approximately 4.3 at 20 °C (Table 1). The magnitude of the fluorescence quenching in the absence of ATPγS was slightly smaller (approximately 56%). However, if ATPγS is added at the end of the titration, the fluorescence intensity decreases to that found when it is present from the beginning, as indicated by the downward arrow in Figure 4 (inset).

Thermodynamic Analysis of TyrR−DNA Binding. The temperature dependence of the association constant in the presence and absence of ATPγS is shown in Figure 5. The data are plotted as $R \ln K_L$ versus absolute temperature, so that the method of Clarke and Glew (*26*) can be used to determine the standard free-energy change (ΔG°), the standard enthalpy change (ΔH°), and the standard heat capacity change at constant pressure (ΔC°_p) for the interaction at a reference temperature θ (see Appendix). This approach has the advantage over conventional van't Hoff analysis that the fitting parameters ΔG°_θ, ΔH°_θ, and $\Delta C^\circ_{p\theta}$ are

Table 2: Thermodynamic Parameters for the Interaction of TyrR with 9F30A/30B at 20 °C

ATPγS	$R \ln K_L$	$\Delta C^\circ_{p\theta}$ (kJ mol^{-1} K^{-1})	ΔG°_θ (kJ mol^{-1})	ΔH°_θ (kJ mol^{-1})	$T\Delta S^\circ_\theta$ [a] (kJ mol^{-1})
present[b]	134.09	-1.03 ± 0.43	-39.32 ± 0.09	37.16 ± 1.84	76.40
absent[c]	121.97	0	-35.73 ± 0.09	57.41 ± 3.13	93.14

[a] $T\Delta S^\circ_\theta$ was calculated using the relationship $T\Delta S^\circ_\theta = -\Delta G^\circ_\theta + \Delta H^\circ_\theta$. [b] Values of the thermodynamic parameters $\Delta C^\circ_{p\theta}$, ΔG°_θ, and ΔH°_θ were obtained by fitting the $R \ln K_L$ versus absolute temperature data shown in Figure 5 to the Clarke and Glew equation. [c] Data were analyzed as above, except that the value of $\Delta C^\circ_{p\theta}$ was constrained to 0.

independent of each other (*27*). The reference temperature θ was chosen as 293.2 K (20 °C), as this was the midpoint of the temperature range over which binding was studied. Values of ΔG°_θ and ΔH°_θ obtained from the Clarke and Glew analysis were used to calculate the standard entropy change for the interaction (expressed as $T\Delta S^\circ_\theta$) using the relationship $T\Delta S^\circ_\theta = -\Delta G^\circ_\theta + \Delta H^\circ_\theta$. A summary of the thermodynamic parameters for the binding of TyrR to 9F30A/30B at 20 °C is presented in Table 2.

In the absence of ATPγS, the plot of $R \ln K_L$ versus absolute temperature was linear within experimental error (Figure 5). Attempts to fit the data according to the Clarke and Glew method to extract a finite value for the standard heat capacity change resulted in a value with a high associated error (0.97 ± 0.85 kJ mol^{-1} K^{-1}), indicating failure to fit to this model. The broken line in Figure 5 shows that the data can be adequately fitted to eq 12 assuming that $\Delta C^\circ_{p\theta} = 0$. Separation of ΔG°_θ into its enthalpic and entropic contributions shows that the interaction is primarily entropically driven at 20 °C (Table 2).

In the presence of saturating levels of ATPγS, binding was also an endothermic process over the temperature range used (Figure 5). However, the Clarke and Glew plot displayed less temperature dependence and was nonlinear. Fitting the data to eq 12 provides a $\Delta C^\circ_{p\theta}$ value of -1.03 ± 0.43 kJ mol^{-1} K^{-1}. Binding is still entropically driven at 20 °C, but the more negative value of ΔG°_θ (reflecting the ATPγS-induced 4.3-fold tighter binding) is due to a favorable decrease in ΔH°_θ (-20.3 kJ mol^{-1}), which overcomes the unfavorable decrease in $T\Delta S^\circ_\theta$ (-16.7 kJ mol^{-1}).

In an attempt to broaden the temperature range used for the thermodynamic analysis of the TyrR-DNA interaction, fluorescence titrations were conducted at 37.5 and 40 °C in the presence and absence of ATPγS (data not shown). In addition to the relatively poor fits of the titration data to eq 4 (especially at 40 °C), the Clarke and Glew plots appeared discontinuous after 35 °C (308.2 K), with $R\,ln K_L$ decreasing sharply from 35 to 40 °C. This behavior is most likely due to TyrR denaturation and justifies the choice of 35 °C as the upper limit for this study.

The Dependence of TyrR−DNA Binding on Monovalent Cation Concentration. Fluorescence titrations were conducted at various KCl concentrations to determine the contribution made by the displacement of DNA-associated cations to the TyrR-DNA interaction. The association constants governing protein−DNA binding (K_{ass}) are generally found to decrease with increasing salt concentration (*28*). When measured in buffers containing a single species of monovalent cation (M^+), log K_{ass} is typically a linear function of log [M^+]. The slope of such a plot yields the number of cations ($Z\psi$) displaced from the DNA upon protein binding, and the ordinate intercept (extrapolated to 1 M M^+) yields the salt-independent association constant (K°_{ass}) (see Appendix) (*28*, *29*).

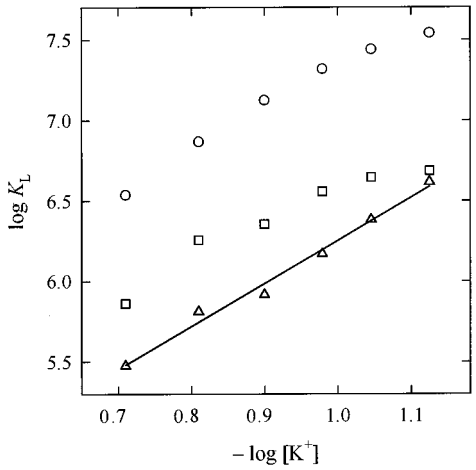

FIGURE 6: Effect of monovalent cation concentration on TyrR-DNA equilibria. The K_L values shown in Table 3 were converted to log K_L data and plotted as a function of the negative logarithm of the total potassium ion concentration. The K_L values were determined from fluorescence titrations of 9F30A/30B (50 nM) with TyrR at 20 °C in buffer I/J mixtures containing the desired potassium ion concentration (see Experimental Procedures). The symbols refer to data obtained in buffer I/J alone (△), in buffer I/J supplemented with 10 mM $MgCl_2$ (□), and in buffer I/J supplemented with 10 mM $MgCl_2$ and 200 μM ATPγS (○). The continuous line is the best fit of the data to eq 14 (see Appendix), which provided values for K°_L and Z of $3.86 \pm 0.02 \times 10^3$ M^{-1} and 3.03 ± 0.17, respectively.

As predicted by polyelectrolyte theory, log K_L was a linear function of log [K^+] when binding was studied in the absence of ATPγS and $MgCl_2$ (i.e., in buffer containing only K^+) (Figure 6, Table 3). The Z value of 3.03 ± 0.17 obtained from the fit of the data to eq 14 (see Appendix) indicates that three ionic interactions are formed upon association of TyrR with 9F30A/30B under these conditions. Since the contributions made to log K_L by nonionic and ionic interactions are described by the quantities log K°_L and $Z\psi$ log [M^+], respectively (see Appendix), knowledge of log K°_L enables calculation of the percent contribution ionic and nonionic interactions make to binding. Thus, the log K°_L value of 3.59 ± 0.14 determined from this analysis suggests that ionic interactions contribute approximately 46% to the binding equilibrium at 75 mM K^+, decreasing to about 35% at 195 mM K^+. In this analysis, [K^+] refers to the total potassium ion concentration, calculated assuming complete dissociation of KCl and K_2HPO_4. This represents a close approximation of [K^+], since a small proportion of potassium will remain bound to orthophosphate (*30*).

In the presence of a fixed concentration of divalent cations (M^{2+}), log K_{ass} displays a nonlinear dependence on log [M^+] due to competition between M^{2+} and the binding protein for

Table 3: Dependence of the TyrR−9F30A/30B Interaction on Potassium Ion Concentration under Different Solution Conditions

	K_L (M^{-1})			
$[K^+]$ (mM)[a]	+ATPγS[b]	−ATPγS[c]	−$MgCl_2$[d]	$FI_i^{(K^+)}/FI_i^{(K^+ + Mg^{2+})}$ (%)[e]
75	$3.47 \pm 0.07 \times 10^7$	$4.85 \pm 0.11 \times 10^6$	$4.13 \pm 0.06 \times 10^6$	78.9
90	$2.75 \pm 0.06 \times 10^7$	$4.43 \pm 0.06 \times 10^6$	$2.42 \pm 0.25 \times 10^6$	80.4
105	$2.08 \pm 0.06 \times 10^7$	$3.61 \pm 0.05 \times 10^6$	$1.48 \pm 0.04 \times 10^6$	89.5
126	$1.33 \pm 0.01 \times 10^7$	$2.27 \pm 0.07 \times 10^6$	$8.26 \pm 0.26 \times 10^5$	91.4
155	$7.38 \pm 0.09 \times 10^6$	$1.81 \pm 0.03 \times 10^6$	$6.49 \pm 0.16 \times 10^5$	96.9
195	$3.46 \pm 0.05 \times 10^6$	$7.29 \pm 0.12 \times 10^5$	$3.00 \pm 0.09 \times 10^5$	99.1

[a] $[K^+]$ calculated as the sum of $[KCl] + 2[K_2HPO_4]$. [b] Fluorescence titrations were performed at 20 °C in the desired buffer I/J mixture (see Experimental Procedures) containing 10 mM $MgCl_2$ and 200 μM ATPγS. [c] Fluorescence titrations were performed as in footnote *b*, but in the absence of ATPγS. [d] Fluorescence titrations were performed as in footnote *c*, but in the absence of $MgCl_2$. [e] The initial fluorescence intensity of 9F30A/30B (before the addition of TyrR) under the conditions described in footnote *d* ($FI_i^{(K^+)}$) is expressed as a percentage of that under the conditions described in footnote *c* ($FI_i^{(K^+ + Mg^{2+})}$).

DNA. Thus, a third parameter that defines the association constant for the M^{2+}−DNA interaction ($K^{M^{2+}-DNA}$) is required in addition to Z and K_{ass}° to describe data of this type (*29*, *31*, *32*). The procedure used to fit the log K_{ass} versus log $[M^+]$ data obtained in a mixed M^+/M^{2+} buffer involves using values of Z and K_{ass}° obtained in the absence of M^{2+}, and allowing $K^{M^{2+}-DNA}$ to be an adjustable parameter since this is itself a strong function of $[M^+]$ (*31*).

Plots of log K_L versus log $[K^+]$ for the TyrR-DNA interaction in the presence of and absence of ATPγS (i.e., both in the presence of Mg^{2+}) are also presented in Figure 6. As expected, log K_L exhibited a nonlinear dependence on log $[K^+]$ due to the interaction being studied in a mixed K^+/Mg^{2+} buffer. In both the presence and absence of ATPγS, the curvature is most evident at low $[K^+]$, when more Mg^{2+} is associated with the DNA, and consequently the competition between Mg^{2+} and TyrR for the DNA is greatest. Although TyrR binding is tighter in the presence of ATPγS at all $[K^+]$ values examined (Table 3, Figure 6), normalization reveals that both plots exhibit very similar curvature (not shown). This suggests that the same number of ionic interactions occur in the unliganded and ATPγS-liganded TyrR-9F30A/30B complexes. Interestingly, the salt dependence of the TyrR-9F30A/30B interaction in the mixed K^+/Mg^{2+} buffer also deviates from the behavior predicted in the model above. A comparison of the data obtained in the presence and absence of $MgCl_2$ (both in the absence of ATPγS) reveals that Mg^{2+} contributes to an enhancement of binding (Table 3, Figure 6). Due to this added effect of Mg^{2+}, further analyses of these data were not pursued.

The Effect of Fluorescein Labeling on the TyrR−DNA Interaction. A comparison between the interaction of TyrR with the labeled (9F30A/30B) and unlabeled (30A/30B) oligonucleotides was made to determine the effect of the conjugated fluorescein chromophore on TyrR binding. Gel shift titrations were employed to qualitatively assess the relative affinities of the labeled and unlabeled acceptors for TyrR. In these experiments the respective oligonucleotides were held at a fixed concentration (0.5 μM) and titrated with TyrR over the concentration range 0−5 μM, in the presence and absence of ATPγS. Relative affinities were judged according to three criteria: (i) the TyrR concentration at which an electrophoretic band representing the complex was first observed, (ii) the concentration of TyrR required for oligonucleotide saturation (i.e., the disappearance of the free DNA species), and (iii) whether the complex dissociated during electrophoretic separation as evidenced by a smeared trailing edge of the complex band.

The gel shift titration shown in Figure 7A is for 9F30A/30B (lanes 1−7) and 30A/30B (lanes 8−14) in the absence of ATPγS. The TyrR−9F30A/30B complex was first discerned at 2 μM TyrR (lane 4). However, the concentrations of TyrR used in this experiment were insufficient to saturate the oligonucleotide, and there is some evidence of dissociation of the complex during electrophoresis (lanes 4−7). In contrast, TyrR−30A/30B complexes were detected at all TyrR concentrations (lanes 9−14), with 30A/30B essentially saturated at 5 μM TyrR (lane 14). Dissociation of the complex was also observed (lanes 9−14).

Figure 7B shows the gel shift titration of 9F30A/30B (lanes 1−7) and 30A/30B (lanes 8−14) conducted in the presence of ATPγS. The TyrR concentration at which the TyrR−9F30A/30B complex was first observed was 2 μM (lane 4), this also being the TyrR concentration at which the oligonucleotide was saturated. Dissociation of the TyrR−9F30A/30B complex is evident in lanes 4−7. The addition of 2 μM TyrR was also saturating with respect to 30A/30B (lane 11). However, the TyrR-30A/30B complex was initially observed at 0.5 μM TyrR (lane 9), and did not dissociate during the experiment. The data presented in Figure 7, parts A and B, indicate that TyrR binds to 30A/30B with a higher affinity than it does to 9F30A/30B and that this stronger binding to the unlabeled species persists in the presence of ATPγS.

Competitive fluorescence titrations were performed to obtain accurate values of the association constants K_L and K_U, which govern the binding of TyrR to 9F30A/30B and 30A/30B, respectively. The rigor of the procedure used to determine these binding parameters (see Appendix) was demonstrated by the analysis of synthetic data sets (not shown). For the purpose of this discussion, we shall treat the unlabeled oligonucleotide as the competitor for the binding of TyrR to the labeled oligonucleotide. These titrations were carried out at 20 °C in the presence and absence of ATPγS and involved the addition of TyrR to mixtures of the labeled and unlabeled oligonucleotides. The concentration of the 30A/30B competitor was either above or below that of the fixed concentration of 9F30A/30B.

A competitive fluorescence titration in the absence of ATPγS is shown in Figure 7C, using 9F30A/30B concentrations of 20.7 nM and 30A/30B concentrations of 9.1 nM (circles) and 90.0 nM (squares). Assuming a 1:1 stoichiometry for both complexes, the data were globally fitted to a modified version of eq 4 (continuous lines), yielding values of $2.22 \pm 0.01 \times 10^6$ M^{-1} for K_L and $1.38 \pm 0.65 \times 10^8$

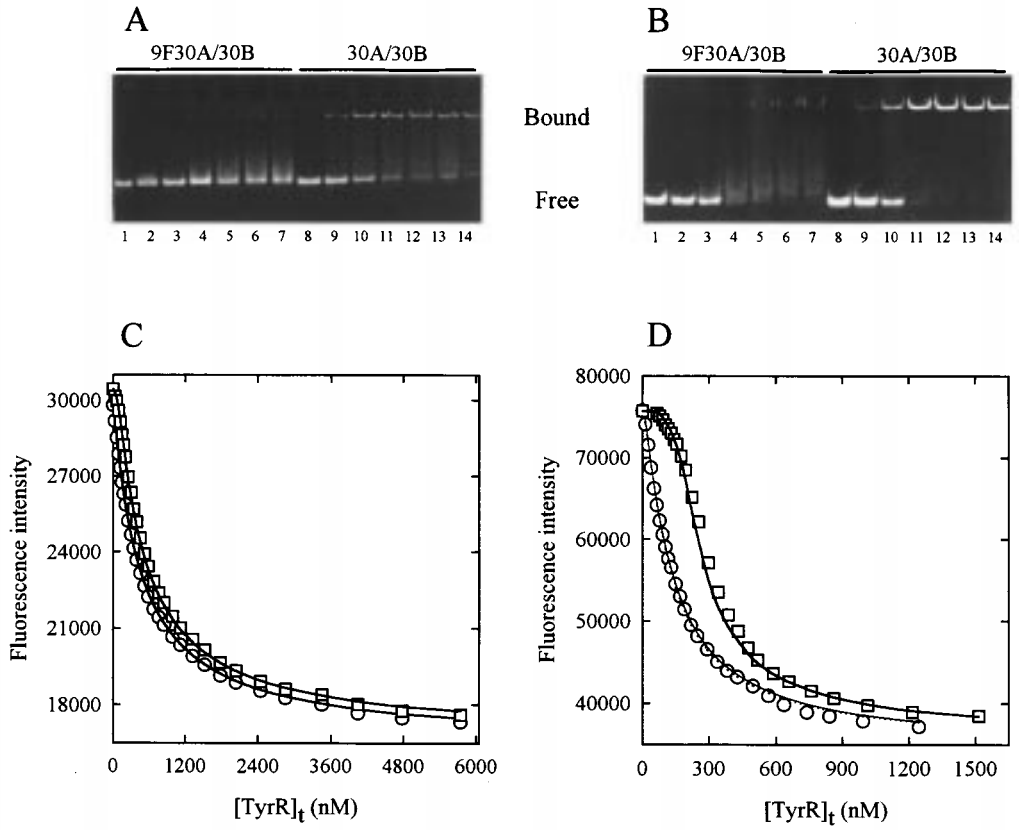

FIGURE 7: Binding of TyrR to labeled versus unlabeled DNA. PAGE analysis: 10 μL reaction mixtures of buffer F containing 0.5 μM oligonucleotide, 10 mM $MgCl_2$, 10% glycerol, and TyrR (0−5 μM) were electrophoresed in the presence and absence of ATPγS on a 7.5% polyacrylamide gel in 1 × TBE for 1 h at a 15 mA constant current. Following electrophoresis, the gels were stained and photographed as described in Experimental Procedures. Part A: gel shift titration of 9F30A/30B (lanes 1−7) and 30A/30B (lanes 8−14) in the absence of ATPγS. For each set of seven lanes (indicated by the lines above the gel), from left to right the TyrR concentration was 0, 0.25, 0.5, 1, 2, 3.5, and 5 μM, respectively. The relative positions of the bound and free DNA species are also indicated. Part B: as for A except that reaction mixtures contained 200 μM ATPγS. Competitive fluorescence titrations: fluorescence titrations were performed at 20 °C as described in Experimental Procedures except that cuvettes contained mixtures of 9F30A/30B and 30A/30B in buffer F supplemented with 10 mM $MgCl_2$, ±ATPγS. Part C: solutions containing 20.7 nM 9F30A/30B plus 9.1 nM 30A/30B (○) and 20.7 nM 9F30A/30B plus 90 nM 30A/30B (□) were titrated with TyrR in the absence of ATPγS. The continuous lines represent the best global fit of the data to a modified form of eq 4 (see Appendix) which provided values for the association constants K_L and K_U of 2.22 ± 0.01 × 10^6 M^{-1} and 1.38 ± 0.65 × 10^8 M^{-1}, respectively. Part D: solutions containing 50 nM 9F30A/30B plus 12.8 nM 30A/30B (○) and 50 nM 9F30A/30B plus 132.4 nM 30A/30B (□) were titrated with TyrR in the presence of 200 μM ATPγS. The continuous lines represent the best global fit of the data as above (K_L = 9.57 ± 0.23 × 10^6 M^{-1} and K_U = 3.01 ± 3.96 × 10^{10} M^{-1}). The broken line is the best fit as described above for the mixture containing 50 nM 9F30A/30B and 12.8 nM 30A/30B (K_L = 1.01 ± 0.01 × 10^7 M^{-1} and K_U = 3.16 ± 2.11 × 10^8 M^{-1}).

M^{-1} for K_U (see Appendix). The value of K_L compares well with that measured in the absence of competitor (Table 1).

Figure 7D depicts a competitive fluorescence titration in the presence of ATPγS using 9F30A/30B concentrations of 50 nM and competitor concentrations of 12.8 nM (circles) and 132.4 nM (squares). The data were analyzed by the procedure outlined above (continuous lines), giving values for K_L of 9.57 ± 0.23 × 10^6 M^{-1} and for K_U of 3.01 ± 3.96 × 10^{10} M^{-1}. The value of K_L agrees reasonably with that determined in the absence of 30A/30B (Table 1). However, the high associated error for K_U indicates difficulty in fitting this parameter. Individual analysis of the mixture containing 50 nM 9F30A/30B and 12.8 nM 30A/30B (Figure 7D; broken line) provided a K_L value of 1.01 ± 0.01 × 10^7 M^{-1}, again close to that reported in Table 1, but the value obtained for K_U was significantly lower (3.16 ± 2.11 × 10^8 M^{-1}). The inability to find a unique solution for K_U suggests stoichiometric binding of TyrR to 30A/30B under the conditions used, with the latter estimate of K_U probably approaching its actual value. The results of these competitive titrations support the gel shift data and indicate tighter binding of TyrR to the unlabeled oligonucleotide. Although the high 30A/30B concentrations used in the presence of ATPγS precluded accurate determination of K_U, these experiments also demonstrated ATPγS-enhanced binding of TyrR to the unlabeled oligonucleotide.

Analysis of TyrR−DNA Binding by Circular Dichroism. The TyrR−DNA interaction was examined by circular dichroism spectroscopy to determine whether TyrR binding induces a conformational change in the DNA. In these experiments the unlabeled oligonucleotide 30A/30B was used instead of 9F30A/30B to avoid contribution of the fluorescein chromophore to the CD signal.

The CD spectra of 30A/30B and TyrR recorded in the absence of ATPγS are shown in Figure 8. The oligonucleotide exhibited negative and positive bands at 247 and 282 nm, respectively, a feature that is characteristic of the B-DNA structure. At the concentrations used, TyrR exhibited negative ellipticity below 250 nm but, compared to the oligonucleotide, made a negligible contribution in the region 255−300 nm. Because of this difference in the spectral contributions of the oligonucleotide and TyrR, perturbations

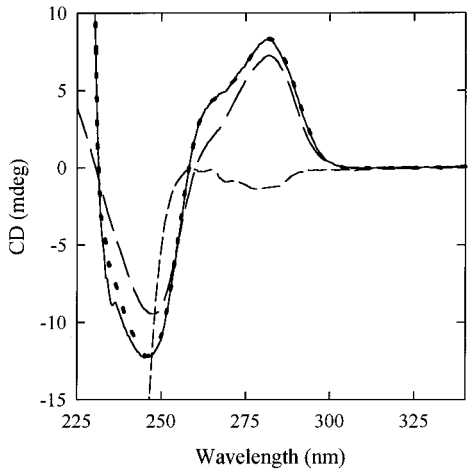

FIGURE 8: TyrR−DNA binding monitored by circular dichroism spectroscopy. Circular dichroism spectra of 10 μM 30A/30B (− − −), 50 μM TyrR (- - -), 10 μM 30A/30B plus 50 μM TyrR (•••) (all in buffer F containing 10 mM $MgCl_2$), and 10 μM 30A/30B plus 50 μM TyrR in buffer F containing 10 mM $MgCl_2$ and 200 μM ATPγS (—). Samples were incubated at 20 °C and scanned at 0.5 nm/min on an Aviv Model 62 DS instrument using 0.1 cm path length quartz cells.

of the positive DNA band observed upon the addition of TyrR may be attributed to changes in DNA structure. A conformational change in 30A/30B resulting from TyrR binding is evident from the CD spectrum of the 30A/30B−TyrR mixture (Figure 8), where the positive DNA band increased in magnitude and developed a distinct shoulder around 264 nm.

Individual CD spectra of 30A/30B and TyrR measured in the presence of ATPγS (not shown) did not differ significantly from those described above. Interestingly, the spectrum of the 30A/30B−TyrR mixture measured in the presence of ATPγS (Figure 8) was virtually identical to that in the absence of ATPγS. As the high reactant concentrations used in both mixtures (10 μM 30A/30B and 50 μM TyrR) would favor saturation of the oligonucleotide with TyrR, these results suggest that the conformational change in the oligonucleotide brought about by TyrR binding is independent of the binding of ATPγS to the protein.

DISCUSSION

Although TyrR boxes are defined as 22 bp elements (*2*), DNase I footprinting experiments show that approximately 26 bp are protected by the TyrR dimer (*33*). Indeed, the weak interaction observed between TyrR and 22 bp oligonucleotides containing a TyrR box is strengthened by extending either side of the binding site with wild-type sequences (*20*). In previous studies oligonucleotide 42mers have been used to examine the binding of dimeric and hexameric TyrR. Oligonucleotides of this length are particularly useful for this purpose, since the hexamer makes contacts with DNA residues lying outside the 26 bp region protected by the dimer (*20*). As the current investigation is concerned only with the dimer-DNA interaction, the use of a shorter 30 bp oligonucleotide was considered more convenient.

The intrinsic fluorescence of TyrR is insensitive to DNA binding; therefore it was necessary to conjugate an extrinsic probe to the DNA to enable fluorescence detection of the interaction. Fluorescein was chosen because of its high quantum yield in aqueous solvents. Fluorescence footprinting studies using 42mers have shown that fluorescein labeling of the thymine residue on the 3′ side of the invariant guanine of the consensus sequence (see Introduction) results in an appreciable perturbation of the fluorescence emission concomitant with dimer binding (*20*). On the basis of this information, the corresponding thymine residue in the 30A oligonucleotide was labeled (Figure 1), and the interaction of the 9F30A/30B duplex with TyrR was studied using fluorescence titrations under a range of solution conditions.

It is possible to compare the binding of TyrR to the aforementioned 42mer (15F42A/42B) and to 9F30A/30B from fluorescence titrations carried out under the same conditions (20 °C, in buffer F containing 200 μM ATPγS, 10 mM $MgCl_2$, and 50 nM oligonucleotide). Surprisingly, the 59% quenching of 9F30A/30B fluorescence observed at saturation with TyrR is inconsistent with the 60% enhancement of 15F42A/42B fluorescence under the same circumstances. In addition, TyrR appears have a significantly lower affinity for 9F30A/30B (1.01×10^7 M^{-1}) than it does for 15F42A/42B (upper limit of 9.09×10^8 M^{-1}). Although a definitive explanation is not available at present, these marked discrepancies are probably due to differences in the chemistries of the reagents used to prepare the labeled oligonucleotides. This seems feasible, since different preparations of the 5-(3-aminoprop-1-yn-1-yl)-2′-deoxyuridine phosphoramidite were incorporated into the two oligonucleotides that were themselves synthesized on separate occasions and labeled with different batches of FITC. On the basis of further binding experiments with 15F42A/42B, we consider that the 9F30A/30B oligonucleotide used in this investigation is the more appropriate species for probing TyrR-DNA equilibria. We offer the following reasons. First, the effect of ATP(γS) in strengthening TyrR-DNA binding is clearly evident for the interaction of TyrR with 9F30A/30B (Figure 4, inset), but not for that of TyrR with 15F42A/42B (data not shown). Second, the TyrR−9F30A/30B interaction exhibits the behavior predicted for a genuine interacting system, in that the association constant is independent of the acceptor concentration and the binding becomes less stoichiometric as the acceptor concentration is decreased (Figure 2). Conversely, the characteristically stoichiometric appearance of the binding curve produced by titration of 15F42A/42B with TyrR (*20*) remains unchanged upon 10-fold dilution of 15F42A/42B to 5 nM (data not shown). This behavior places considerable doubt on the assertion that 9.09×10^8 M^{-1} represents the upper limit of the association constant for the TyrR-15F42A/42B interaction. Third, 42A/42B was resynthesized with the modified 5-(3-aminoprop-1-yn-1-yl)-2′-deoxyuridine at position 15 and labeled with FITC to produce 15F42A/42B. Titration of newly prepared 15F42A/42B with TyrR (20 °C, in buffer F containing 200 μM ATPγS, 10 mM $MgCl_2$, and 50 nM 15F42A/42B) gave rise to a smooth quenching curve (data not shown). The association constant and degree of fluorescence quenching obtained upon fitting the data to eq 4 (1.12×10^7 M^{-1} and 57%, respectively) were essentially identical to those obtained for the titration of 9F30A/30B under the same conditions (Table 1). Importantly, when the titration of 15F42A/42B was conducted in the absence of ATPγS (data

not shown), the association constant and degree of quenching decreased to 2.55×10^6 M^{-1} and 54%, respectively.

Binding data were analyzed assuming a stoichiometry of one TyrR dimer per 9F30A/30B acceptor. The validity of this assumption is supported by simulation of a 1:1 TyrR−9F30A/30B interaction under stoichiometric conditions (Figure 2C), and by ultracentrifugation studies which found a 1:1 stoichiometry for the interaction of TyrR dimer with a 42mer containing the same recognition sequence (*34*). Using this model, the binding parameters K_L and F_B (see Appendix) were obtained by direct fitting of the raw data, rather than by analysis of transformed data. The binding constant determined with different preparations of the labeled 30mer at 20 °C and in the presence of ATPγS was the same within experimental error as that reported in Table 1 (i.e., compare $1.01 \pm 0.01 \times 10^7$ M^{-1} (Table 1) to $1.20 \pm 0.06 \times 10^7$ M^{-1} (Figure 2)). Furthermore, different preparations of the TyrR protein had negligible effect on the value of the association constant measured under these conditions (data not shown).

The lower thermal stability of TyrR ($T_m = 40$ °C) relative to that of 9F30A/30B ($T_m = 61.4$ °C) (Figure 3) determined the choice of 35 °C as the upper limit for studying the thermodynamics of their interaction. The presence of ATPγS increased the affinity of TyrR for 9F30A/30B at all temperatures, with the effect being more pronounced at lower temperatures (Table 1). ATP-mediated enhancement is presumably an allosteric phenomenon, whereby the binding of ATP to its site within the central domain of each TyrR monomer unit is linked to a conformational change in the C-terminal region, resulting in a better fit between the helix-turn-helix motifs and the DNA of the strong box. This model implies that the unliganded and ATPγS-liganded TyrR−9F30A/30B complexes have different three-dimensional structures. Evidence of this is provided by the magnitude of fluorescence quenching in the presence (59%) and absence (56%) of ATPγS, which indicates a different environment of the fluorescein probe in each complex. An effect of ATP in mediating a conformational change in TyrR has been demonstrated by limited proteolysis studies (*7*). These studies show that while ATP binding confers protection against trypsin digestion at a site within the central domain, the region linking the central domain to the C-terminal domain becomes more susceptible to proteolytic cleavage. A similar effect of ATP has also been observed with NtrC, a protein structurally related to TyrR (*35*). In this case the binding of ATPγS results in protection of the central domain against trypsin digestion but has no effect on the rate of digestion in other parts of the protein.

TyrR−DNA binding, expressed as $R \ln K_L$, (Figure 5), exhibited a linear dependence on the absolute temperature in the absence of ATPγS, indicating that the binding enthalpy is independent of temperature. In contrast, the presence of ATPγS resulted in a nonlinear dependence of $R \ln K_L$ on the absolute temperature. Such behavior is frequently observed for site-specific binding of proteins to DNA and originates from the dependence of the binding enthalpy on temperature. The derivative of this function, $(\partial \Delta H^\circ/\partial T)_p$, is equal to ΔC_p°. For these systems, ΔC_p° is commonly a large negative quantity and is attributed to conformational changes in the protein (primarily the burial of nonpolar surface area) upon binding to DNA (*28*, *36*). Thus, the $\Delta C_{p\theta}^\circ$ value of -1.03 ± 0.43 kJ mol^{-1} K^{-1} recovered from the Clarke and Glew analysis (Table 2) is consistent with a conformational change in the TyrR−ATPγS complex accompanying DNA binding. The inability to extract a finite value for $\Delta C_{p\theta}^\circ$ for the interaction in the absence of ATPγS suggests either that TyrR does not undergo a conformational change involving the removal of nonpolar surface under these conditions or that such a change is too small to detect using this approach. The value of $\Delta C_{p\theta}^\circ$ determined in the presence of ATPγS is comparable to ΔC_p° values obtained for the site-specific DNA binding of other regulatory proteins containing the helix-turn-helix motif, such as the *lac* and *trp* repressors (-3.77 ± 0.42 and -2.26 ± 0.42 kJ mol^{-1} K^{-1}, respectively) (*36*−*38*). The relatively large uncertainty associated with ΔC_p° for these systems is mainly due to the fact that this parameter is estimated indirectly, as the second derivative of a Clarke and Glew or van't Hoff plot. In the case of a weak protein−nucleic acid interaction, ΔC_p° may be resolved with greater accuracy using a technique such as titration microcalorimetry, where the binding enthalpy can be measured directly at a range of experimental temperatures.

On a weight basis, ΔC_p° accompanying protein denaturation is substantially greater than for the melting of DNA ($\approx$0.38−0.63 compared to $\approx$0.17−0.25 J g^{-1} K^{-1}). It has therefore been suggested that the major contribution to ΔC_p° for a specific protein−DNA interaction originates from the protein rather than the DNA and specifically from a reduction in the water-accessible nonpolar surface area of the protein on complex formation (*28*). Nevertheless, a distortion of the DNA structure induced by TyrR binding might also contribute to the favorable $\Delta C_{p\theta}^\circ$ for the interaction. The marked change in the positive CD band of 30A/30B upon addition of TyrR and ATPγS (Figure 8) indeed indicates that binding of the TyrR−ATPγS complex alters the DNA structure. However, the fact that a virtually identical spectral change was produced in the absence of ATPγS suggests that the DNA undergoes the same conformational change upon binding either TyrR or the TyrR−ATPγS complex. Therefore, the negative standard heat capacity change and the enhanced binding observed in the presence of ATPγS can be accounted for solely by a conformational change in the TyrR−ATPγS complex accompanying DNA binding. Unfortunately, such a change in the conformation of TyrR cannot be monitored easily by CD spectroscopy due to the significant contribution of the oligonucleotide to the ellipticity below 250 nm.

The other thermodynamic parameters derived from the Clarke and Glew analysis also distinguish binding in the presence of ATPγS from that in its absence (Table 2). At the reference temperature (20 °C), the greater stability of the ATPγS-liganded TyrR−9F30A/30B complex is demonstrated by a $\Delta\Delta G_\theta^\circ$ value of -3.59 kJ mol^{-1}. Interestingly, binding exhibits enthalpy−entropy compensation regardless of the involvement of ATPγS; that is, in each case the positive and hence unfavorable ΔH_θ° term is offset by a more positive $T\Delta S_\theta^\circ$ term, resulting in a negative value of ΔG_θ°. Contributions to the positive entropic terms may come from processes occurring at the protein−DNA interface, such as the release of protein-bound water molecules (resulting from the formation of hydrophobic interactions) and the release of monovalent cations associated with the phosphate backbone of the DNA. The latter notion is supported by the dependence of the TyrR−9F30A/30B

interaction on monovalent cation concentration, which shows that binding is accompanied by the release of two to three potassium ions (Figure 6). Although this information was obtained in the absence of ATPγS and magnesium ions, it suggests that this process plays an important role in TyrR−DNA binding. The more favorable ΔG°_θ value determined in the presence of ATPγS relative to that in its absence is primarily due to the difference in ΔH°_θ rather than $T\Delta S^\circ_\theta$. The average enthalpy of hydrogen bond formation ranges from 12 to 24 kJ mol^{-1} (*39*); thus the enthalpy loss observed in the presence of ATPγS (−20.3 kJ mol^{-1}) may result from the formation of one or two extra hydrogen bonds in the TyrR−DNA complex. The existence of extra hydrogen bonds would also confer a greater degree of order to this system, and may explain the accompanying loss in $T\Delta S^\circ_\theta$ of 16.7 kJ mol^{-1}.

One limitation of conjugating the fluorescein probe within the TyrR box is that it weakens the TyrR-DNA interaction (Figures 7A and B). This may be due to the probe sterically hindering binding, given that it is positioned in the major groove of the DNA next to one of the essential GC basepairs (Figure 1). The quenching of fluorescein fluorescence concomitant with TyrR binding suggests that there is contact between the protein and the probe in the complex. Steric hindrance of binding may be exacerbated by charge repulsion between the dianionic probe and the negatively charged DNA backbone, which would result in the probe being oriented away from the backbone and into the solution. Indeed, this may explain why the binding of TyrR to 9F30A/30B is tighter in buffer containing both K^+ and Mg^{2+} relative to that in buffer containing only K^+ (Table 3, Figure 6). Binding of Mg^{2+} to fluorescein may either partially or completely neutralize its negative charges, thereby increasing the configurational flexibility of the probe and rendering the binding site more accessible to the protein. The greater fluorescence of the free 9F30A/30B conjugate (i.e., prior to the addition of TyrR) observed in the mixed K^+/Mg^{2+} buffer (Table 3) suggests that Mg^{2+} stabilizes the probe in its excited state and provides evidence of Mg^{2+}−fluorescein binding. Slight unwinding of the 9F30A/30B duplex caused by the introduction of the negatively charged probe (Figure 3) may also inhibit TyrR recognition. Conventional 5′ labeling has the potential to overcome the problem of weakened binding, since it removes the probe from the binding site, but in so doing eliminates any influence of the protein in the quantum yield of the fluorophore. In this case binding would have to be monitored by an increase in fluorescence anisotropy. Unfortunately, accurate measurement of the interaction is more difficult using this approach, since the difference in anisotropy between the bound and free DNA species is relatively small. This is primarily due to the fact that the rotational correlation time of the DNA (<10 ns) exceeds the average lifetime of the probe (2−4 ns).

The inhibitory effect of the fluorescein probe precludes determination of the "absolute" thermodynamic parameters that characterize the TyrR-DNA interaction. An important question is whether the effect of ATP (ATPγS) on the interaction is similar, in thermodynamic terms, for both the labeled and unlabeled systems. There is only limited data available on this question. Bailey et al. (*34*) used analytical ultracentrifugation at 20 °C to show that ATPγS caused a 3.5-fold increase in the association constant for the binding of TyrR to a 42-bp oligonucleotide containing the same recognition sequence as that used in the present investigation. In their experiments, the subsaturating concentrations of ATPγS used (30 μM compared to 200 μM in the present study) would slightly underestimate the magnitude of the ATP effect. However, the 3.5-fold enhancement observed for unlabeled DNA agrees well with the 4.3-fold enhancement found for labeled DNA in the current study (Table 1). A study by Kwok et al. (*4*) of *Rsa*I protection of the strong box of the *tyrP* operator at 37 °C showed that saturating ATP concentrations (200 μM) caused a 3−4-fold enhancement of the TyrR-DNA interaction. Given the semiquantitative nature of the electrophoretic assay used in these studies, the lower limit of the enhancement (3-fold) is in good agreement with the 2.4-fold enhancement found at 35 °C in the present study (Table 1). Thus, it is probable that the effect of ATP on ΔH°_θ and $\Delta C^\circ_{p\theta}$ is similar for the labeled and unlabeled DNA systems, given that these parameters are respectively the first and second derivatives of the plot of the natural logarithm of the binding constant against the absolute temperature. Correspondingly, the values of the association constants (and hence ΔG°_θ) obtained with labeled DNA would be offset from their "absolute" values by a constant factor across the temperature range used in this study.

Competitive fluorescence titrations involving the addition of TyrR to mixtures of 9F30A/30B and 30A/30B enabled a quantitative determination of the extent to which fluorescent labeling interferes with TyrR binding (Figure 7C,D). The data obtained in the absence of ATPγS were well described by the competitive binding model (see Appendix) with the values extracted for K_L and K_U ($2.22 \pm 0.01 \times 10^6$ M^{-1} and $1.38 \pm 0.65 \times 10^8$ M^{-1}, respectively) indicating an approximately 60-fold stronger interaction of the protein with the unlabeled DNA. The concentrations of the 30A/30B competitor used in the presence of ATPγS were too high to permit accurate resolution of K_U. However, the K_L and K_U values recovered from the analysis of the competitive titration containing the lower concentration of competitor ($1.01 \pm 0.01 \times 10^7$ M^{-1} and $3.16 \pm 2.11 \times 10^8$ M^{-1}, respectively) suggest that the affinity of TyrR for the unlabeled DNA is at least 30-fold tighter under these conditions. In both the presence and absence of ATPγS, the binding constants describing the TyrR−9F30A/30B interaction were in close agreement with those obtained in the absence of competitor (Table 1), reflecting the near-zero correlation between the fitting parameters K_L and K_U. As expected, ATPγS-mediated enhancement of the interaction was also observed for the TyrR−30A/30B interaction. With judicious choice of experimental conditions, the competitive binding approach may be extended to investigate the effect variables such as DNA length, supercoiling, etc. have on the interaction with TyrR. In particular, this technique could be applied to measuring the strength of TyrR interactions with different operators, since this is likely to be an important factor, along with box position, in determining the extent to which different operons are regulated.

APPENDIX

Analysis of Binding Data. The binding of the TyrR dimer (D) to 9F30A/30B (L) to yield a 1:1 complex (LD) is controlled by the equilibrium constant K_L:

$$L + D \overset{K_L}{\rightleftharpoons} LD \qquad K_L = [LD]/[L][D] \tag{1}$$

where square brackets denote molar concentrations. When titrations are performed in the presence of saturating concentrations of ATPγS (200 μM), it is assumed that D is complexed with 2 molecules of ATPγS ($D^{ATP\gamma S_2}$), and that this species binds to L to yield the ternary complex $LD^{ATP\gamma S_2}$. For convenience the superscript ATPγS_2 is not adopted in the proceeding discussion; however, this notation is implied for all species of D under these conditions.

The fractional saturation of L is defined by the binding function *r*,

$$r = K_L[D]/(1 + K_L[D]) \tag{2}$$

which can also be written in terms of fluorescence intensities

$$r = (FI - F_F)/(F_B - F_F) \tag{3}$$

where *FI* is the measured fluorescence intensity, and F_F and F_B are the fluorescence intensities of L and LD, respectively. Substitution of eq 2 into eq 3 and subsequent rearrangement yields

$$FI = F_F + \frac{(F_B - F_F)(K_L[D])}{1 + K_L[D]} \tag{4}$$

where [D] is the solution to a quadratic, solved in terms of K_L and the total concentrations of L and D

$$[D] = \frac{-(1+ K_L([L]_t - [D]_t)) + \sqrt{(1 + K_L([L]_t - [D]_t))^2 + 4K_L[D]_t}}{2K_L} \tag{5}$$

where $[L]_t$ and $[D]_t$ refer to the total concentrations of L and D, respectively. Data were analyzed by nonlinear regression using eq 4, with *FI*, $[L]_t$, and $[D]_t$ as variables and K_L and F_B as fitting parameters.

Analysis of Competitive Binding Data. Competitive titrations involved the addition of D to solutions containing both L and 30A/30B (U). It is also assumed that D binds to U, yielding UD:

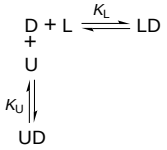

where K_U is the binding constant governing the binding of D to U. The total concentration of L may be written as

$$[L]_t = [L](1 + K_L[D]),$$

which rearranges to give $[D] = ([L]_t - [L])/K_L[L]$ (6)

Similar rearrangement of the equations for $[U]_t$ and $[D]_t$ gives

$$[U] = [U]_t/1 + K_U[D] \tag{7}$$

and

$$[D] = [D]_t/(1 + K_L[L] + K_U[U]) \tag{8}$$

Substituting eq 6 into eq 7 gives

$$[U] = \frac{[U]_t}{1 + K_U([L]_t - [L])K_L[L]} \tag{9}$$

Substituting eq 9 into eq 8 gives

$$[D] = \frac{[D]_t}{1 + K_L[L] + \dfrac{K_U([U]_t K_L[L])}{K_U[L]_t - [L](K_U - K_L)}} \tag{10}$$

F_B was obtained from the ordinate intercept of a plot of $1/FI$ versus $1/[D]_t$. [L] was then calculated as

$$[L] = [L]_t\left(1 - \frac{FI - F_F}{F_B - F_F}\right) \tag{11}$$

Equation 10 was substituted into eq 4 and the data analyzed as described above, with *FI*, $[L]_t$, [L], $[U]_t$, and $[D]_t$ as variables and K_L and K_U as fitting parameters.

Thermodynamic Analysis of TyrR−DNA Binding. The temperature dependence of K_L was analyzed by the Clarke and Glew equation (*26*) using a reference temperature θ:

$$R \ln K_L = -\frac{\Delta G^\circ_\theta}{\theta} + \Delta H^\circ_\theta\left(\frac{1}{\theta} + \frac{1}{T}\right) + \Delta C^\circ_{p\theta}\left[\frac{\theta}{T} - 1 + \ln\left(\frac{T}{\theta}\right)\right] \tag{12}$$

where ΔG°_θ is the standard free-energy change, ΔH°_θ is the standard enthalpy change, and $\Delta C^\circ_{p\theta}$ is the standard heat capacity change of binding, all at temperature θ. *R* is the gas constant and *T* is the absolute temperature.

Effect of Monovalent Cation Concentration on TyrR−DNA Binding. In dilute electrolyte solutions, the structural charge density of DNA (in this case 9F30A/30B) is neutralized principally by the binding of monovalent cations (M^+). The fraction of M^+ thermodynamically associated with the DNA per phosphate (ψ) is found to be 0.88 ± 0.05 for double-stranded B-DNA (*28*). Thus, 9F30A/30B can be described as the weak electrolyte ($M^+_\psi L^-$). In the absence of ATPγS and $MgCl_2$, the TyrR−9F30A/30B interaction may be modeled as a simple cation exchange process. TyrR is assumed to be a *Z*-valent oligocation (D^{Z+}), which interacts with *Z* phosphates on $M^+_\psi L^-$, resulting in a reduction in the structural charge density of the DNA and the release of $Z\psi$ monovalent cations from the DNA to the bulk solution (*28*, *31*).

$$M^+_\psi L^- + D^{Z+} \overset{K^\circ_L}{\rightleftharpoons} LD + Z\psi\, M^+ \quad K^\circ_L = \frac{[LD]Z\psi[M^+]}{[L][D]} \tag{13}$$

Combining the equilibrium expressions for K_L and K°_L (eqs 1 and 13, respectively), the dependence of K_L on $[M^+]$ is given by

$$\log K_L = \log K^\circ_L - Z\psi \log [M^+] \tag{14}$$

According to this treatment, the ordinate intercept ($\log K^\circ_L$) of a plot of $\log K_L$ versus $\log [M^+]$ provides a measure of the association constant at the 1 M M^+ pseudostandard state (i.e., in the absence of any ionic interactions). The slope

($Z\psi$) yields the number of monovalent cations released from 9F30A/30B upon the binding of TyrR (*28*).

ACKNOWLEDGMENT

We thank Robert Chan for performing the CD measurements, Don Winzor for assistance with the competitive binding theory, and Leanne Bailey for critical review of the manuscript.

REFERENCES

1. Pittard, A. J. (1996) in *Escherichia coli and Salmonella: Cellular and Molecular Biology* (Neidhardt, F. C., Curtiss, R., III, Ingraham, J. L., Lin, E. C. C., Low, K. B., Magasanik, B., Reznikoff, W. S., Riley, M., Schaechter, M., and Umbarger, H. E., Eds.) pp 458−484, ASM Press, Washington, D.C.
2. Pittard, A. J., and Davidson, B. E. (1991) *Mol. Microbiol. 5*, 1585−1592.
3. Yang, J., Ganesan, S., Sarsero, J., and Pittard A. J. (1993) *J. Bacteriol. 175*, 1767−1776.
4. Kwok, T., Yang, J., Pittard, A. J., Wilson, T. J., and Davidson, B. E. (1995) *Mol. Microbiol. 17*, 471−481.
5. Argaet, V. P., Wilson, T. J., and Davidson, B. E. (1994) *J. Biol. Chem. 269*, 5171−5178.
6. Wilson, T. J., Maroudas, P., Howlett, G. J., and Davidson, B. E. (1994) *J. Mol. Biol. 238*, 308−319.
7. Cui, J., and Somerville, R. L. (1993) *J. Biol. Chem. 268*, 5040−5047.
8. Cui, J., and Somerville, R. L. (1993) *J. Bacteriol. 175*, 1777−1784.
9. Yang, J., Camakaris, H., and Pittard, A. J. (1993) *J. Bacteriol. 175*, 6372−6375.
10. Wilson, T. J., Argaet, V. P., Howlett, G. J., and Davidson, B. E. (1995) *Mol. Microbiol. 17*, 483−492.
11. Walker, J. E., Saraste, M., Runswick, M. J., and Gay, N. J. (1982) *EMBO J. 8*, 945−951.
12. Henikoff, S., and Wallace, J. C. (1988) *Nucleic Acids. Res. 16*, 6191−6204.
13. Morett, E., and Segovia, L. (1993) *J. Bacteriol. 175*, 6067−6074.
14. Bochner, B. R., and Ames, B. N. (1982) *J. Biol. Chem. 257*, 9759−9769.
15. Andrews, A. E., Lawley, B., and Pittard, A. J. (1991) *J. Bacteriol. 173*, 5068−5078.
16. Sarsero, J. P., and Pittard, A. J. (1991) *J. Bacteriol. 173*, 7701−7704.
17. Lawley, B., and Pittard, A. J. (1994) *J. Bacteriol. 176*, 6921−6930.
18. Andrews, A. E., Dickson, B., Lawley, B., Cobbett, C., and Pittard, A. J. (1991) *J. Bacteriol.* 173, 5079−5085.
19. Hagmar, P., Bailey, M., Tong, G., Haralambidis, J., Sawyer, W. H., and Davidson, B. E. (1995) *Biochim. Biophys. Acta 1244*, 259−268.
20. Bailey, M., Hagmar, P., Millar, D. P., Davidson, B. E., Tong, G., Haralambidis, J., and Sawyer, W. H. (1995) *Biochemistry 34*, 15802−15812.
21. Applied Biosystems Inc. (1989) *User Bulletin No. 1*, Foster City, CA.
22. Ruth, J. L. (1991) in *Oligonucleotides and Analogues*: *A Practical Approach* (Eckstein, F., Ed.) pp 255−282, IRL Press, Oxford, New York, and Tokyo.
23. Eckstein, F. (1985) *Annu. Rev. Biochem. 54*, 367−402.
24. Cui, J., Ni, L., and Somerville, R. L. (1993) *J. Biol. Chem. 268*, 13023−13025.
25. Breslauer, K. J., Sturtevant, J. M., and Tinocco, I., Jr. (1975) *J. Mol. Biol. 99*, 549−565.
26. Clarke, C. W., and Glew, D. N. (1966) *Trans. Faraday Soc. 62*, 539−547.
27. Kim, S. J., Tsukiyama, T., Lewis, M. S., and Wu, C. (1994) *Protein Sci. 3*, 1040−1051.
28. Record, M. T., Jr., Ha, J.-H., and Fisher, M. A. (1991) *Methods Enzymol. 208*, 291−343.
29. Record, M. T., Jr., Anderson, C. F., and Lohman, T. M. (1978) *Q. Rev. Biophys. 11*, 103−178.
30. Smith, R. M., and Alberty, R. A. (1956) *J. Phys. Chem. 60*, 180−184.
31. Strauss, H. S., Burgess, R. R., and Record, M. T., Jr. (1980) *Biochemistry 19*, 3504−3515.
32. Lohman, T. M., deHaseth, P. L., and Record, T. M., Jr. (1980) *Biochemistry 19*, 3522−3530.
33. Baseggio, N., Davies, W. D., and Davidson, B. E. (1990) *J. Bacteriol. 172*, 2547−2557.
34. Bailey, M. F., Davidson, B. E., Minton, A. P., Sawyer, W. H., and Howlett, G. J. (1996) *J. Mol. Biol. 263*, 671−684.
35. Farez-Vidal, M. E., Wilson, T. J., Davidson, B. E., Howlett, G. J., Austin, S., and Dixon, R. A. (1996) *Mol. Microbiol. 22*, 779−788.
36. Ha, J.-H., Spolar, R. S., and Record, M. T., Jr. (1989) *J. Mol. Biol. 209*, 801−816.
37. Whitson, P. A., Olson, J. S., and Matthews, K. S. (1986) *Biochemistry 25*, 3852−3858.
38. Jin, L., Yang, J., and Carey, J. (1993) *Biochemistry 32*, 7302−7309.
39. Kyte, J. (1995) in *Structure in Protein Chemistry*, pp 147−196, Garland Publishing, Inc., New York and London.
40. Cornish, E. C., Argyropoulos, V. P., Pittard, A. J., and Davidson, B. E. (1986) *J. Biol. Chem. 261*, 403−410.
41. Klonis, N., and Sawyer, W. H. (1996) *J. Fluoresc. 6*, 147−157.

BI972854A